Electronic Supplementary Material (ESI) for Analyst.

Supplementary Information

For

A Portable Molecularly Imprinted Polymer-Modified Microchip Sensor for Rapid Detection of Perfluorooctanoic Acid

Yingmei Wei[a], Hongjie Liu[b,c], Shaopeng Wang[a], Kefu Yu*[a,d], Liwei Wang*[a,c,d]

[a] *School of Marine Sciences, Coral Reef Research Center of China, Guangxi Laboratory on the Study of Coral Reefs in the South China Sea, Guangxi University, Nanning, 530004, PR China*

[b] *School of Chemistry and Chemical Engineering, Guangxi University, Nanning 530004, P.R. China*

[c] *Guangxi Key Laboratory of Processing for Non-ferrous Metallic and Featured Materials, Guangxi University, Nanning, 530004, PR China*

[d] *Southern Marine Science and Engineering Guangdong Laboratory (Zhuhai), Zhuhai, 519080, PR China*

***Corresponding Authors**

Email address: wangliwei0427@163.com (A/Prof. L. W. Wang);

kefuyu@scsio.ac.cn (Prof. K. F. Yu)

1. Experimental Section

1.1 Materials and Reagents

perfluorooctanoic acid (PFOA, 95%), o-phenylenediamine (o-PD, >98%), perfluorooctanesulfonic acid potassium salt (PFOS, ⩾98%), Perfluorobutanoic acid (PFBA, 98%), Perfluorobutanesulfonic acid (PFBS, 98%), Tris-HCl, humic acid and dopamine hydrochloride were purchased from Sigma-Aldrich; $CuSO_4·5H_2O$, $CoCl_2·6H_2O$, $Ni(NO_3)_2·6H_2O$, glucose, NaOH were purchased from Sinopharm Chemical Reagent Co. Ltd. Ethanol was purchased from Chengdu Chron Chemicals Co. Ltd. Urea were purchased from Macklin (Shanghai, China); Fresh lemon juice was bought from local market.

1.2 Preparation of the Cu_2O Precursor

A slight modification was made to the literature-based synthesis procedure for the Cu_2O precursor[S1]. Firstly, 10 mL of fresh lemon juice was diluted with 30 mL of DI water under thorough stirring, which was put into a 50 mL stainless steel autoclave and hydrothermal treatment for 5 h in an oven at 180°C. Then, a syringe filter with a pore size of 0.22 μm was used to filter the reddish-brown solution. The acquired solution was named "solution A" and stored at 4°C. Typically, 0.5 g of $CuSO_4·5H_2O$ and 7.5 mL of "solution A" were stirred into 42.5 mL of DI water to be dissolved; then 10 mL of NaOH (1 M) was added after the above-mentioned solution was heated to 60°C, and then 10 mL of glucose solution (0.3 M) was injected quickly; after remaining at 60°C for 3 h, the products were centrifugated, and washed several times with DI water and ethanol. Finally, the Cu_2O precursor products were dried overnight at 80°C. The relevant chemical reactions are as follow:

$$2CuSO_4 \cdot 5H_2O + 4NaOH + 2C_6H_{12}O_6 + 2C_5H_5O_5 \rightarrow 2Cu_2O + 2H_2O + 4NaHSO_4 + 2CO_2 \quad (S1)$$

1.3 Preparation of the Cu_2O@C Precursor

After homogeneously dispersing 320 mg of the Cu_2O template by sonication for 30 min in Tris-buffer solution (100 mL, 10 mM), dopamine hydrochloride (160 mg)

was added and continually stirred for 3 h. Centrifugation was used to collect the Cu_2O@PDA product, which was then washed three times with DI water and ethanol before being dried overnight at 60°C. Then, with a heating rate of 2°C min^{-1}, the obtained Cu_2O@PDA product was annealed in N_2 at 500°C for 3 h to get a Cu_2O@C precursor [S2].

1.4 Preparation of the Cu_2O@C@$NiCo_2O_4$ Composite

The obtained Cu_2O@C precursor (100 mg) was dispersed into 15 mL of ethanol and sonicated for 10 min. Then, 20 mM of $Co(NO_3)_2 \cdot 6H_2O$, 10 mM of $Ni(NO_3)_2 \cdot 6H_2O$, 90 mM of urea and 30 mL of DI water were added, and the solution was bathed in 90 °C with vigorous magnetic stirring for 6 h. After that, centrifugation was used to collect the product, which was washed several times with ethanol and DI water, and then dried overnight at 60°C, followed by 2 h of air annealing at 300°C with a heating rate of 2°C min^{-1} to obtain the final electrode material of Cu_2O@C@$NiCo_2O_4$ [S3]. The corresponding chemical reaction can be expressed as follows[S4]:

$$2NH_2(CO)NH_2 + 5H_2O \rightarrow 4NH_4^+ + 2OH^- + CO_3^{2-} + CO_2 \quad (S2)$$

$$Ni^{2+} + 2Co^{2+} + 3OH^- + 1.5CO_3^{2-} \rightarrow NiCo_2(CO_3)_{1.5}(OH)_3 \quad (S3)$$

$$2NiCo_2(CO_3)_{1.5}(OH)_3 + O_2 \rightarrow 2NiCo_2O_4 + 3CO_2 + 3H_2O \quad (S4)$$

1.5 Fabrication process of the FR-4 Au chip MIP-PFOA electrode

The FR-4 Au chip electrodes was commercial electrode bought from Guangzhou Yuxin Sensor Technology Co., Ltd., and the fabrication process of the FR-4 Au chip MIP-PFOA electrode can be seen in **Figure S1**, which is similar to the fabrication of in the Au electrode in **Scheme 1**. Moreover, the detailed parameters of the FR-4 Au chip electrode was listed in **Table S1**.

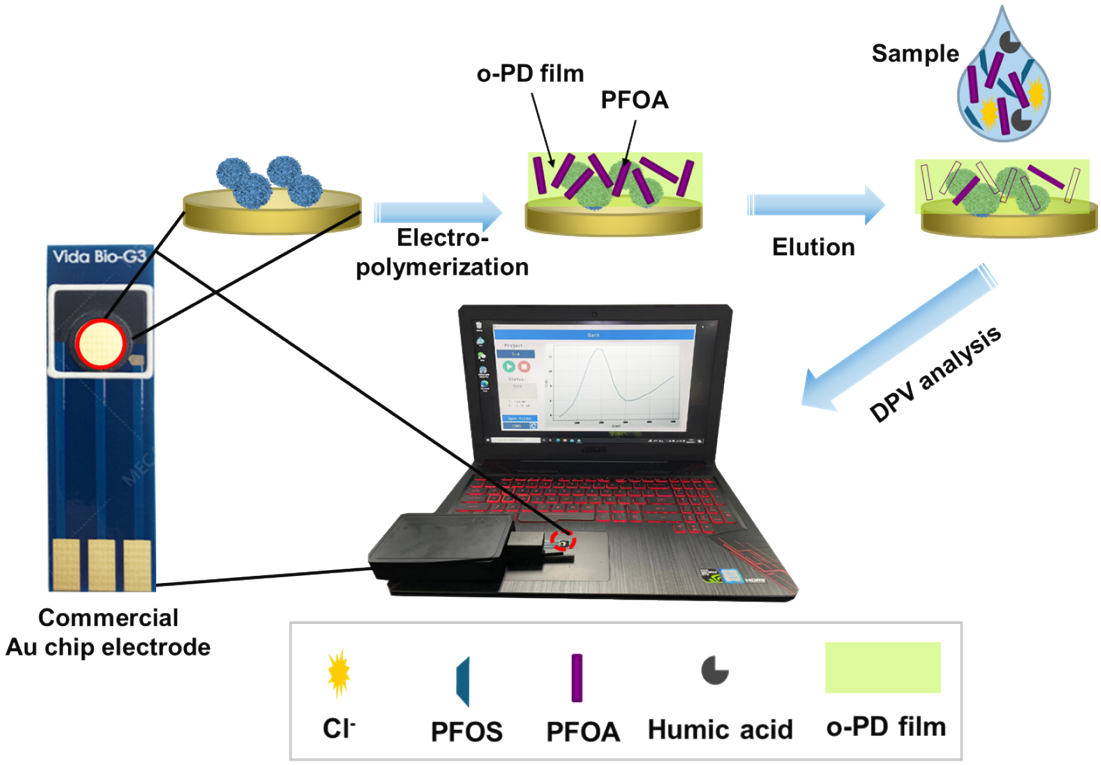

Figure S1. The fabrication process of the FR-4 Au chip MIP-PFOA electrode.

Table S1. The detailed parameters of the FR-4 Au chip electrode

Material	FR-4 epoxy resin substrate
Working electrode	Au electrode
Counter electrode	Glass electrode
Reference electrode	Ag/AgCl electrode
Size (mm^2)	40 x 12.5
Surface (μm)	Au 0.08
Conductive inner layer (μm)	Cu 35.0
Work area (mm^2)	23.75

1.6 Details of Randel's Equivalent Circuit Model

In the inset of **Figure 1f**, R_{ct}, R_s, Z_w, and C_{dl} are combined into an equivalent circuit model to describe the interaction between an electrode and a solutions [S5,S6] R_{ct} represents charge transfer resistance, which is the resistance to electron transfer caused

by chemical reactions and mass transfer in electrochemical reactions. It is commonly used to describe the electrochemical reaction at the electrode surface. The larger the value of R_{ct}, the more significant the effect of potential on the charge transfer rate. R_s represents electrolyte resistance, which is the resistance to ion transport in a water solution. The existence of R_s is mainly due to the interaction between the charges on the electrode surface and ions, leading to changes in ion concentration with distance from the electrode surface and resulting in resistance. Z_w represents warburg impedance, which is arises from the diffusion of species in the electrochemical system and is modeled by the Warburg element (or Warburg component), which is a resistance due to the diffusion of electrolytic species and is often represented as a sloping linear segment. The slope of the Warburg element also changes with the movement of the electrolyte and the diffusion rates of different species. C_{dl} represents the double layer capacitance of the electrode and is modeled as a capacitance consisting of two layers of dielectric.

The combination of these elements in an equivalent circuit model forms a complex circuit model that can help in understanding the complex interaction between both electrode surface and electrolyte. Generally, the ohmic resistance (Rs) with the origin of the axis to the beginning of the semicircle shows the internal resistance of the electrodes and electrolyte. The charge transfers impedance (Rct) is illustrated by the obvious semicircle in the intermediate frequency region. Warburg impedance (Zw) is named as the solid-state diffusion resistance, which can be reflected in the slope line at low-frequency regions. The constant phase elements (C_{dl}) are ascribed to the double-layer capacitance.

As for the equivalent circuit model for MIP-based sensor, the model can be modified as follow:

In the EIS equivalent circuit model, both C_{dl} and CPE are components used to describe the double layer capacitance. C_{dl} represents the double layer capacitance and

is modeled as a capacitance consisting of two layers of dielectric. It is commonly used to describe charge transfer at the surface of a solid electrode and electrolyte capacitance. C_{dl} can be considered as a thin capacitance, and its capacitance value changes with variation in potential. CPE, on the other hand, is a capacitance resistor element that can be thought of as a capacitance reflecting the complexity of charge accumulation and exchange between the electrode and the solution, and non-ideal nature of the surface. It is typically used to describe non-electrochemical reactions such as surface species adsorption, chemical exchange, or unconventional impedance characteristics. In summary, C_{dl} is typically used to describe the dynamics of charge transfer, while CPE is often used to describe the non-ideal nature of the surface. Furthermore, C_{dl} has a changing capacitance value while CPE has a nonlinear response to voltage or current similar to electrical conductivity.

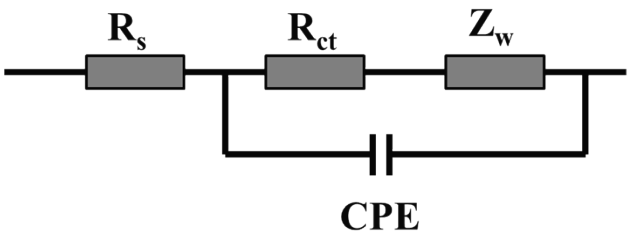

Figure S2. The equivalent circuit model of MIP-based sensor.

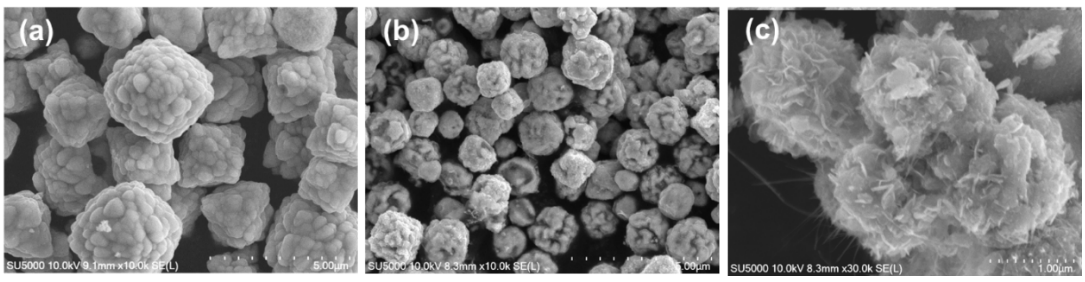

Figure S3. The lower magnified FE-SEM images of (a) Cu_2O, (b) Cu_2O@C and (c) Cu_2O@C@$NiCo_2O_4$.

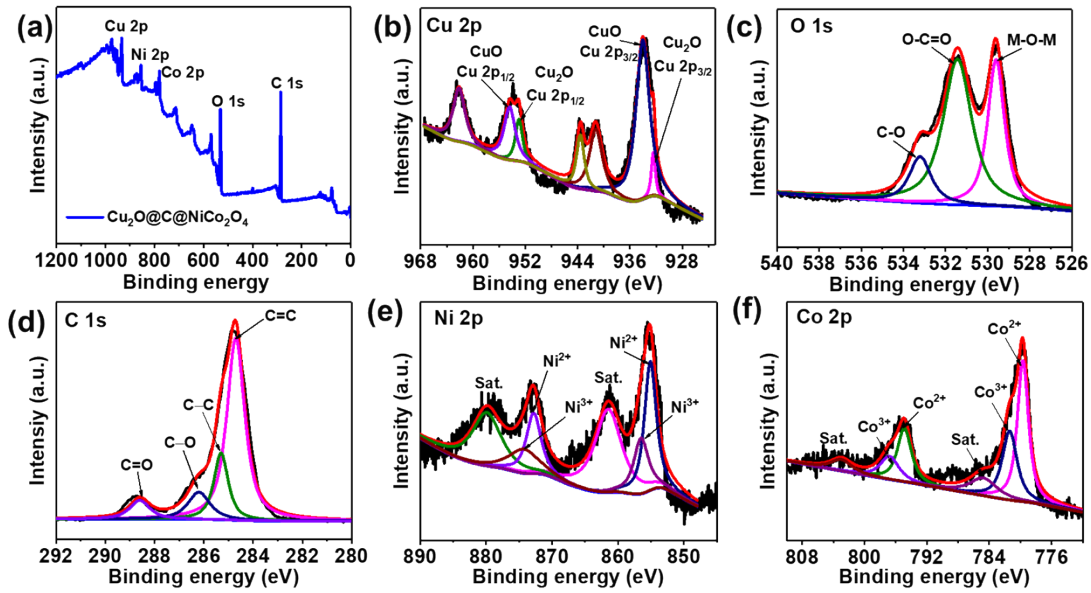

Figure S4. (a) XPS survey spectrum of $Cu_2O@C@NiCo_2O_4$. High resolution XPS spectra of (b) Cu 2p, (c) O 1s, (d) C 1s, (e) Ni 2p and (f) Co 2p in the $Cu_2O@C@NiCo_2O_4$.

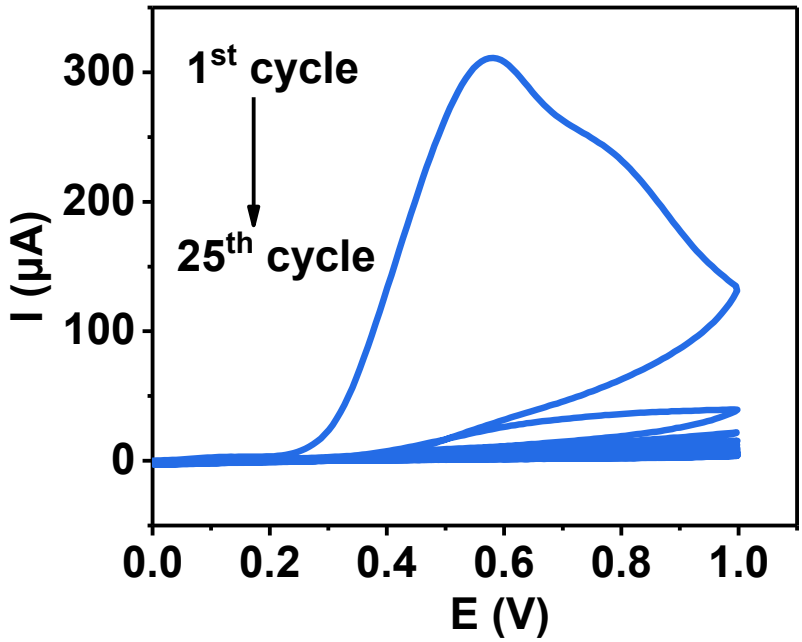

Figure S5. CV of the Au electrode representing oxidative electro-polymerization of 10 mM o-PD in the absence and the presence of 1 mM PFOA in acetate buffer (pH=5.8) and methanol (2:1, v/v) solution over 25 cycles at a scan rate of 200 mV s^{-1}.

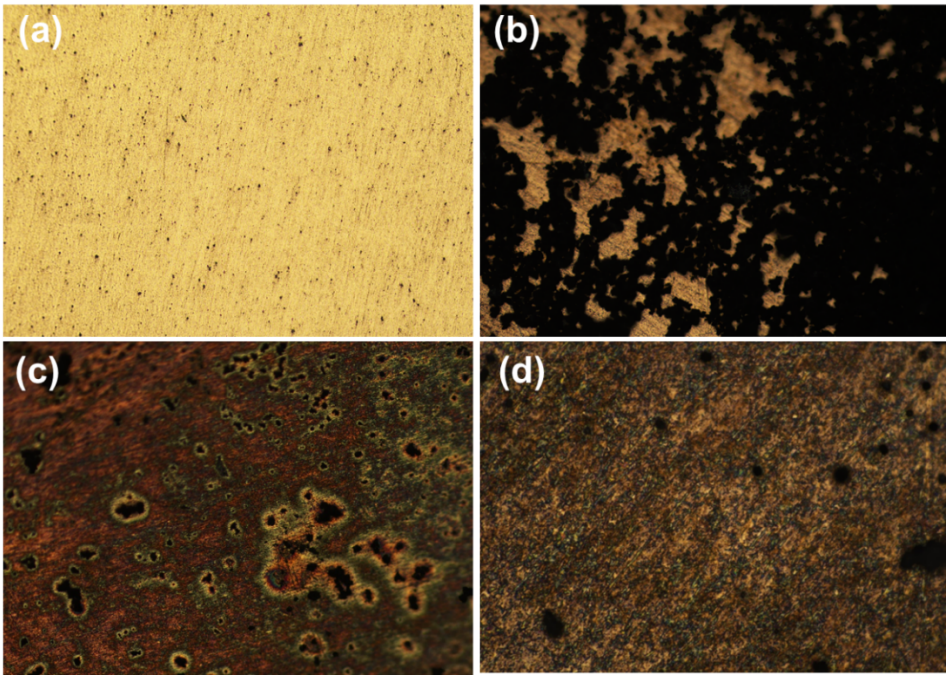

Figure S6. The metallurgical microscope characterizations of (a) bare Au electrode, (b) initial electrode, (c) MIP electrode, and (d) MIP-PFOA electrode.

Table S2. Comparison with other methods for the determination of PFOA and PFOS.

Methods	Need Preconcentration or not	Instrument price	LOD (ng/L)	Analyte	ref
genetically engineered bacterial biosensor	yes	high	10 and 10	PFOS and PFOA	S7
resonance light scattering	yes	low	4557.7	PFOA	S8
surface plasmon resonance	yes	low	130	PFOA	S9
photoluminescence sensing	no	low	10351.75	PFOA	S10
fluorospectrophotometry	no	low	59.9	PFOS	S11
fluorescent sensor	yes	low	6387 and 4886	PFOS and PFOA	S12
Colorimetric	yes	low	1.03×10^5	PFOA	S13
Colorimetric	yes	low	496.88	PFOA	S14
LC-MS	yes	high	231.88 and 265	PFOS and PFOA	S15
nESI-MS	yes	high	11	PFOA	S16
d-SPE-GC–MS	yes	high	2.6	PFOA	S17
MIP sensor	no	low	24.95	PFOA	S18
MIP sensor	no	low	0.08	HFPO-DA	S19
MIP sensor	no	low	1.69	PFOS	S20
MIP sensor	no	low	7.49	PFOS	S21
MIP sensor	no	low	2095.8	PFOS	S22
MIP sensor	no	low	19.96	PFOS	S23
MIP sensor	no	low	41407	PFOS	S24
MIP sensor	no	low	19.47	PFOA	This work

nESI-MS: nano-electrospray ionization mass spectrometry

Table S3. Determination of PFOA in real seawater samples using the MIP-based chip sensor.

Sample	Added (nM)	Found (nM)	Recovery (%)	RSD (%)
1	0.1	0.096	98.7	2.4
2	0.5	0.58	103.8	1.5
3	1	1.02	102.5	3.5

Reference:

S1 G. Muthusankar, M. Sethupathi, S. M. Chen, R. K. Devi, R. Vinoth, G. Gopu, N. Anandhan and N. Sengottuvelan, *Compos. Part B Eng.*, 2019, **174**, 106973.

S2 S. Wang, B. Y. Guan and X. W. Lou, *Energy Environ. Sci.*, 2018, **11**, 306–310.

S3 G. Gao, H. Bin Wu, S. Ding, L. M. Liu and X. W. Lou, *Small*, 2015, **11**, 804–808.

S4 X. Luo, M. Huang, D. He, M. Wang, Y. Zhang and P. Jiang, *Analyst*, 2018, **143**, 2546–2554.

S5 D. Balciunas, D. Plausinaitis, V. Ratautaite, A. Ramanaviciene and A. Ramanavicius, *Talanta*, 2022, **241**, 123252.

S6 D. Wang, J. Wang, J. Zhang, Y. Li, Y. Zhang, Y. Li and B. C. Ye, *Talanta*, 2019, **196**, 479–485.

S7 G. Sunantha and N. Vasudevan, *Sci. Total Environ.*, 2021, **759**, 143544.

S8 F. Zhang, Y. Zheng, J. Liang, S. Long, X. Chen and K. Tan, *Spectrochim. Acta - Part A Mol. Biomol. Spectrosc.*, 2016, **159**, 7–12.

S9 N. Cennamo, G. D'Agostino, G. Porto, A. Biasiolo, C. Perri, F. Arcadio and L. Zeni, *Sensors (Switzerland)*, 2018, **18**, 1–11.

S10 L. Zheng, Y. Zheng, Y. Liu, S. Long, L. Du, J. Liang, C. Huang, M. T. Swihart and K. Tan, *Talanta*, 2019, **194**, 1–6.

S11 J. Liang, X. Deng and K. Tan, *Spectrochim. Acta - Part A Mol. Biomol. Spectrosc.*, 2015, **150**, 772–777.

S12 Z. Cheng, L. Du, P. Zhu, Q. Chen and K. Tan, *Spectrochim. Acta - Part A Mol. Biomol. Spectrosc.*, 2018, **201**, 281–287.

S13 M. Takayose, K. Akamatsu, H. Nawafune, T. Murashima and J. Matsui, *Anal. Lett.*, 2012, **45**, 2856–2864.

S14 C. Fang, X. Zhang, Z. Dong, L. Wang, M. Megharaj and R. Naidu, *Chemosphere*, 2018, **191**, 381–388.

S15 R. Knob, V. Maier, J. Petr, V. Ranc and J. Ševčík, *Electrophoresis*, 2012, **33**, 2159–2166.

S16 P. Suwannakot, F. Lisi, E. Ahmed, K. Liang, R. Babarao, J. J. Gooding and W. A. Donald, *Anal. Chem.*, 2020, **92**, 6900–6908.

S17 S. Y. Ma, J. Wang, L. Fan, H. L. Duan and Z. Q. Zhang, *J. Chromatogr. A*, 2020, **1611**, 460616.

S18 R. Kazemi, E. I. Potts and J. E. Dick, *Anal. Chem.*, 2020, **92**, 10597–10605.

S19 M. W. Glasscott, K. J. Vannoy, R. Kazemi, M. D. Verber and J. E. Dick, *Environ. Sci. Technol. Lett.*, 2020, **7**, 489–495.

S20 R. B. Clark and J. E. Dick, *ACS Sensors*, 2020, **5**, 3591–3598.

S21 D. Lu, D. Z. Zhu, H. Gan, Z. Yao, J. Luo, S. Yu and P. Kurup, *Sensors Actuators B Chem.*, 2022, **352**, 131055.

S22 Y. Gao, W. Gou, W. Zeng, W. Chen, J. Jiang and J. Lu, *Microchem. J.*, 2023, **187**, 108378.

S23 N. Karimian, A. M. Stortini, L. M. Moretto, C. Costantino, S. Bogialli and P. Ugo, *ACS Sensors*, 2018, **3**, 1291–1298.

S24 C. Fang, Z. Chen, M. Megharaj and R. Naidu, *Environ. Technol. Innov.*, 2016, **5**, 52–59.